Variational dynamics as a ground-state problem on a quantum computer

Stefano Barison [1,2,*] Filippo Vicentini [1] Ignacio Cirac [3] and Giuseppe Carleo [1,2]

[1] *Institute of Physics, École Polytechnique Fédérale de Lausanne (EPFL), CH-1015 Lausanne, Switzerland*

[2] *National Centre for Computational Design and Discovery of Novel Materials MARVEL, EPFL, Lausanne, Switzerland*

[3] *Max-Planck-Institut für Quantenoptik, Hans-Kopfermann-Str. 1, 85748 Garching, Germany*

(Received 22 April 2022; accepted 24 October 2022; published 5 December 2022)

We propose a variational quantum algorithm to study the real-time dynamics of quantum systems as a ground-state problem. The method is based on the original proposal of Feynman and Kitaev to encode time into a register of auxiliary qubits. We prepare the Feynman-Kitaev Hamiltonian acting on the composed system as a qubit operator and find an approximate ground state using the variational quantum eigensolver. We apply the algorithm to the study of the dynamics of a transverse-field Ising chain with an increasing number of spins and time steps, proving a favorable scaling in terms of the number of two-qubit gates. Through numerical experiments, we investigate its robustness against noise, showing that the method can be used to evaluate dynamical properties of quantum systems and detect the presence of dynamical quantum phase transitions by measuring Loschmidt echoes.

DOI: 10.1103/PhysRevResearch.4.043161

I. INTRODUCTION

Recent years have seen tremendous developments in the fabrication, control, and deployment of quantum computing systems, and it is now possible to access quantum computing platforms with up to a hundred qubits on the cloud [1–4]. These devices are expected to surpass the capabilities of classical computers in specific tasks such as factorization [5], database search [6], and quantum simulation [7–9].

Among these tasks, quantum simulation was the first envisioned application of quantum computers [10] and has been proven to be of polynomial complexity (bounded-error quantum polynomial time, BQP) on devices making use of quantum resources [11,12]. Due to its potential impact on many different areas of physics [13,14], chemistry [15,16], and materials science [17,18], a significant amount of research has been devoted to such application.

However, the realization of an universal quantum simulator remains far in the future due to the combined effect of limited connectivity and noisy gates: the noise sets a maximum number of operations that can be performed without affecting the fidelity, and the sparse connection graph among qubits increases the total number of physical operations that must be performed to implement an algorithm. As an example, several recent works describing optimized algorithms for quantum dynamics require a number of quantum operations (gates) well beyond the possibility of current hardware to surpass classical capabilities [19–22]. A computational strategy that works around the constraints of the hardware is the use of hybrid quantum-classical algorithms [23–31]. In this approach, the quantum computer is used to perform a subroutine of limited depth, while the whole algorithm is governed by a classical computer. In the context of quantum dynamics, several hybrid algorithms approximating the real-time evolution of a physical quantum system have been proposed [24,27,29–36]. Those algorithms rely on a variational trial state (ansatz) whose parameters θ are optimized classically in order to approximate the desired state.

A remarkably different approach, which has not yet been thoroughly investigated on quantum computers, treats time as a quantum degree of freedom by encoding it into an auxiliary system called the *clock*. In that picture, the state $|\psi(t)\rangle$ at a certain time t is represented as the composite state $|\psi(t)\rangle \otimes |t\rangle$. This approach is of interest because it allows to encode the dynamics of a system into a static superposition of such states, $\sum_t |\psi(t)\rangle \otimes |t\rangle$, and each state $|\psi(t)\rangle$ can be obtained by projecting the clock into the corresponding state $|t\rangle$. Given a time-dependent system, it is possible to construct a Hamiltonian for the joint physical-clock system whose ground state encodes the whole evolution of the original system. Such construction, originally proposed by Feynman and Kitaev [37–40] in the case of a discrete clock and later extended to continuous time [41], is effectively recasting the problem of quantum dynamics into a ground-state problem. This perspective leads to a different classical variational principle [42–44] that allows the application of ground-state techniques from quantum chemistry and condensed-matter physics to quantum dynamics. A similar construction was also recently proposed to address the simulation of time-dependent Hamiltonians [45].

In this work we extend the original idea to perform the variational optimization of the ground state with a hybrid quantum

*stefano.barison@epfl.ch

algorithm. First, we show how to prepare the Feynman-Kitaev Hamiltonian efficiently as a qubit operator. Then, we consider a variational ansatz for the ground state and optimize the circuit parameters using the variational quantum eigensolver (VQE) [23,46,47]. We reiterate that this approach allows us to study quantum dynamics using a wide number of techniques originally developed for ground-state problems. Moreover, it is related to McLachlan's variational principle [42,48], which is suggested to be the most consistent variational principle for quantum simulation [27,29]. Finally, once a variational approximation of the ground state is obtained, we propose to use it to evaluate the dynamical properties of the physical system and detect dynamical quantum phase transitions [49].

The structure of this paper is as follows: In Sec. II we present the Feynman-Kitaev Hamiltonian and its efficient mapping onto a series of qubit operators, while in Sec. III we apply the method to the study of a transverse-field Ising chain, comparing the results to both exact and noisy Trotter simulations. Section IV concludes the paper with some considerations and outlooks on the proposed algorithm.

II. METHODS

In this section we will describe how to construct the Feynman-Kitaev Hamiltonian given a time-evolving physical system and how to apply it in a hybrid quantum algorithm.

A. Feynman-Kitaev Hamiltonian

We consider a quantum system governed by a Hamiltonian $\hat{H}$ acting on the physical Hilbert space $\mathcal{H}_p$. To simplify the discussion, we assume that $\hat{H}$ is time independent, but that is not a requirement. Given the initial state of the system $|\psi(t=0)\rangle$, the state at every time t is $e^{-i\hat{H}t}|\psi(0)\rangle = \hat{U}(t,0)|\psi(0)\rangle$, the formal solution of the time-dependent Schrödinger equation.

The unitary transformations $\hat{U}(t,t') = \hat{U}(t-t')$ form a one-parameter group, therefore we can use the group composition property to write

$$\hat{U}(t,0)|\psi(0)\rangle = \hat{U}(t,t_{n-1})\dots\hat{U}(t_2,t_1)\hat{U}(t_1,0)|\psi(0)\rangle, \quad (1)$$

where we suppose $t = t_n > t_{n-1} > \dots > t_1 > t_0 = 0$. By taking $t_i - t_{i-1} = dt \quad \forall i \in \{1,\dots,n\}$, the expression in Eq. (1) becomes $\hat{U}^n(dt)|\psi(0)\rangle$, namely, we have discretized the time evolution of the system in n equal substeps of length dt.

We then consider an auxiliary clock system $\mathcal{H}_c = \text{span}\{|0\rangle, |1\rangle, \dots |n\rangle\}$ with $\langle i|j\rangle = \delta_{ij} \quad \forall i,j \in \{0,\dots,n\}$. They correspond to the different times $\{t_0, t_1, \dots t_n\}$. We then define the *history state* to be the coherent superposition of the physical states $|\psi(t)\rangle$ at different times in the joint physical-clock system $\mathcal{H} = \mathcal{H}_p \otimes \mathcal{H}_c$,

$$|\Psi\rangle = \frac{1}{\sqrt{n+1}}\sum_{i=0}^{n}\hat{U}^i(dt)|\psi(0)\rangle|i\rangle = \frac{1}{\sqrt{n+1}}\sum_{i=0}^{n}|\psi_i\rangle|i\rangle, \quad (2)$$

where we defined for simplicity $\hat{U}^i(dt)|\psi(0)\rangle = |\psi_i\rangle$. From the history state it is possible to extract the physical state at any time t by projecting on the auxiliary qubits

$$|\psi_i\rangle = \sqrt{n+1}\langle i|\Psi\rangle. \quad (3)$$

We now define the Feynman-Kitaev Hamiltonian $\hat{C}$ as the operator whose ground state corresponds to the history state with energy 0 [10,38]. Similarly to Ref. [42], we present it in a form amenable to implementation on quantum computers. The Hamiltonian can be split into three terms:

$$\hat{C} = \hat{C}_0 + \tfrac{1}{2}(\hat{C}_1 - \hat{C}_2), \quad (4)$$

where

$$\begin{aligned}\hat{C}_0 &= [\hat{\mathbf{I}} - |\psi(0)\rangle\langle\psi(0)|] \otimes |0\rangle\langle 0|,\\ \hat{C}_1 &= \sum_{i=0}^{n-1}\hat{\mathbf{I}}\otimes|i\rangle\langle i| + \hat{\mathbf{I}}\otimes|i+1\rangle\langle i+1|,\\ \hat{C}_2 &= \sum_{i=0}^{n-1}\hat{U}(dt)\otimes|i+1\rangle\langle i| + \hat{U}^\dagger(dt)\otimes|i\rangle\langle i+1|.\end{aligned} \quad (5)$$

$\hat{C}_0$ favors the initial state $|\psi(0)\rangle$ by giving a positive contribution to the energy for any other state. $\hat{C}_1$ and $\hat{C}_2$ encode for the evolution of the physical and auxiliary quantum system through time, by giving a positive contribution to the energy when the state at different times does not evolve according to the unitary operator $\hat{U}(dt)$. We will call $\hat{U}(dt)\otimes|i+1\rangle\langle i|$ the forward unitary and its adjoint the backward unitary. By construction, we have that the energy $E(|\psi\rangle) = \langle\psi|\hat{C}|\psi\rangle \geqslant 0$ for every state $|\psi\rangle$ and the equality holds only for $|\psi\rangle = |\Psi\rangle$.

Considering a state $|\phi\rangle = \sqrt{1-\epsilon^2}|\Psi\rangle + \epsilon|\delta\rangle$ with $\epsilon \approx 0$, $\langle\Psi|\delta\rangle = 0$ so that it is close to the target state, it is possible to show that the infidelity between $|\phi\rangle$ and the target $|\Psi\rangle$ is $1 - F(\phi,\Psi) = \epsilon^2$, where we defined $F(\phi,\Psi) = |\langle\phi|\Psi\rangle|^2$, given $|\phi\rangle$ and $|\Psi\rangle$ pure states. Meanwhile, the energy is given by $E(|\phi\rangle) \approx k\epsilon^2$ for some constant $k \geqslant E_1$, where E_1 is the energy of the first excited state of the Feynman-Kitaev Hamiltonian. The computationally costly infidelity is therefore upper-bounded by the normalized energy $1 - F(\phi,\Psi) \leqslant E(|\phi\rangle)/E_1$, that can thus be used as a convergence metric in variational optimization.

B. Efficient mapping on quantum hardware

We want to encode the history state on the qubits of a quantum computer, therefore we need to find an efficient mapping for the Feynman-Kitaev Hamiltonian onto qubit operators. The physical and auxiliary subsystems are encoded into a different partition of qubits. For the physical system, we will resort to one of the many established mappings [50,51]. The auxiliary register, instead, is a $n+1$-level system, and there are in principle combinatorially many ways to map it to qubits [52]. In this work we considered both the standard binary and the Gray mapping [53] to encode every state $|i\rangle$ into a bit string state. Since n_a binary digits have 2^{n_a} different values, encoding n different time steps requires $n_a = \log_2(n)$ auxiliary qubits using those mappings. The main difference among binary and Gray encoding is how many (qu-)bits must be flipped when going from one time step $|i\rangle$ to the next. Under binary encoding one will eventually need to flip all qubits, such as when going from $|i=3\rangle \leftrightarrow |011\rangle$ to $|i=4\rangle \leftrightarrow |100\rangle$ in the case of $n_a = 3$. Gray code, instead, is built in order to flip only one bit at every step, and therefore the time-step

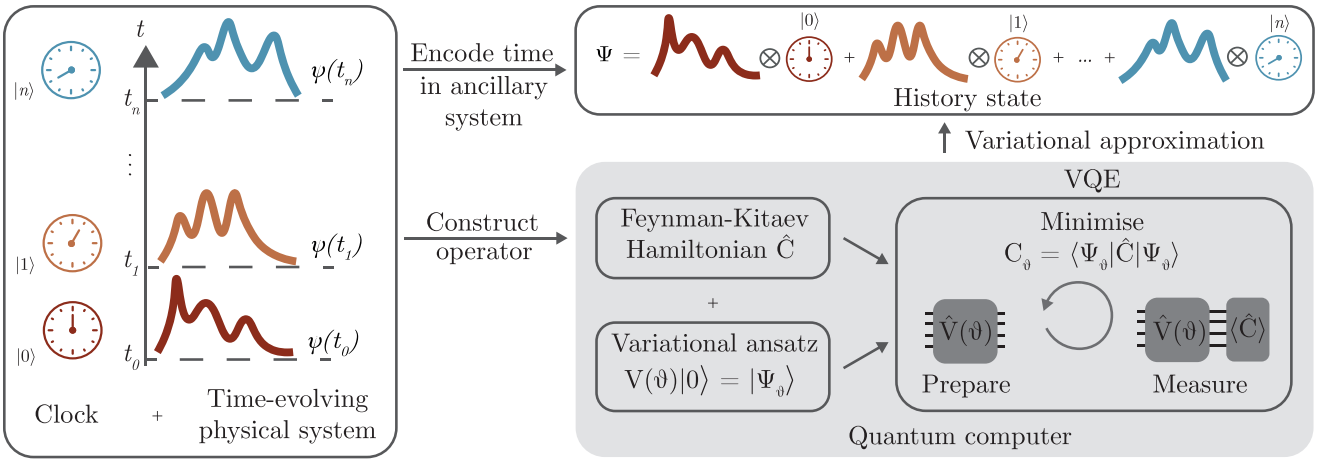

FIG. 1. Sketch of the VFK method. Coupling the physical system to an auxiliary clock system, we can encode an entire time evolution into a time-independent state. We prepare a variational approximation of the history state by measuring the expectation value of the Feynman-Kitaev Hamiltonian and its derivatives on a quantum computer.

operator $|i\rangle\langle i+1|$ can be implemented with a single qubit rotation on one qubit.

Consider the time step $|i\rangle$ and its Gray binary mapping $|x_{n_a}\dots x_2x_1\rangle$, $x_i \in \{0,1\}\ \forall i$. Let x_j be the difference in bits between $|i\rangle$ and $|i+1\rangle$. Then, the auxiliary forward operator has the form

$$|i+1\rangle\langle i| = \left|x_{n_a}\right\rangle\!\left\langle x_{n_a}\right| \otimes \cdots \otimes |\neg x_j\rangle\langle x_j| \otimes \cdots \otimes |x_1\rangle\langle x_1|, \tag{6}$$

where $\neg$ indicates the negation of the bit value. This is a tensor product of operators acting on single qubits. Then, each term is mapped onto qubit operators using the following equalities:

$$\begin{aligned} |x\rangle\langle x| &= \tfrac{1}{2}[\hat{\mathbf{I}} + (-1)^x\hat{\sigma}^z], \\ |\neg x\rangle\langle x| &= \tfrac{1}{2}[\hat{\sigma}^x + (-1)^x i\hat{\sigma}^y], \end{aligned} \tag{7}$$

where $\hat{\sigma}^x$, $\hat{\sigma}^y$, and $\hat{\sigma}^z$ indicate the Pauli operators. The same considerations apply to the backward auxiliary operator and the projectors.

The last term to consider is the time evolution operator $U(dt)$. In general, it is not possible to prepare $\hat{U}(dt)$ exactly in an efficient way if the Hamiltonian contains noncommuting terms. For this reason we will consider the Trotter-Suzuki approximation of the time evolution operator [54,55].

Having shown how to prepare the Feynamn-Kitaev as a qubit operator, we can now use the variational quantum eigensolver (VQE) [23] with such Hamiltonians to optimize the variational parameters of a quantum circuit in order to obtain an approximation of the history state. Considering a unitary variational circuit ansatz $|\Psi_\theta\rangle = \hat{V}(\theta)|0\rangle$, we will use the quantum computer to measure $E_\theta = \langle\Psi_\theta|\hat{C}|\Psi_\theta\rangle$ and its derivatives. Iteratively, a classical processor will determine new values of θ to minimize E_θ. We remark that minimizing E_θ has been proved to be equivalent to the application of McLachlan's variational principle [42,48]. In the following, we will refer to the whole procedure as the variational Feynman-Kitaev (VFK) method.

Once a variational approximation of the history state is obtained, we measure expectation values of observables $\hat{O}$ on the system at time step t using the following equality:

$$\langle\hat{O}(t)\rangle = \langle\psi_t|\hat{O}|\psi_t\rangle \sim \langle\Psi_\theta|[\hat{O}\otimes|t\rangle\langle t|]|\Psi_\theta\rangle. \tag{8}$$

An sketch of the method is shown in Fig. 1, while example applications of the final variational history state can be found in Sec. III.

C. Computational cost on quantum hardware of the Feynman-Kitaev Hamiltonian

In this section we analyze the computational cost of measuring the Feynman-Kitaev Hamiltonian in Eq. (4) on a quantum device. First, we estimate the number of Pauli strings acting on the clock n^c_{Pauli} and on the physical system n^p_{Pauli}. Then, the total number of Pauli strings will be $n^{\text{tot}}_{\text{Pauli}} \leqslant n^p_{\text{Pauli}} * n^c_{\text{Pauli}}$.

Given a number of time steps n, or $n_a = \log_2 n$ auxiliary qubits to encode them, we can determine how many Pauli strings will make up the operators acting on the auxiliary system. The terms in C_0 and C_1 are projectors $|i\rangle\langle i|$ with $i \in \{0,\dots,n\}$, and can be expressed as 2^{n_a} combinations of $\hat{\mathbf{I}}$ and $\hat{\sigma}^z$, as indicated in Eq. (7), that can be measured all at once. On the contrary, C_2 contains the forward and backward unitaries, resulting in $n\log_2 n = n_a 2^{n_a}$ different Pauli strings.

For the physical system, we approximated the time evolution operator with a single Trotter-Suzuki step of size dt. The unitary operation corresponding to a Trotter step is not local if the terms of the physical Hamiltonian do not commute, giving a final number of different Pauli strings exponential in the physical qubits, a behavior that may hinder scalability of the proposed method. For this reason, we have to resort to a different strategy. Consider the m sets of noncommuting operators H_m that constitute the physical Hamiltonian $H = \sum_m H_m$. We can rewrite the operator C_2 as

$$\hat{C}_2 = \sum_{i=0}^{n'-1}\sum_{j=0}^{m-1} \hat{U}_j(dt)\otimes|ij+1\rangle\langle ij| + \hat{U}_j^\dagger(dt)\otimes|ij\rangle\langle ij+1|, \tag{9}$$

where $U_j(dt) = e^{-iH_j dt}$ is the jth set of commuting operators, which can be exactly Trotterized, and $n' = \lfloor\frac{n}{m}\rfloor$. The physical

part of the Feynman-Kitaev Hamiltonian will have m sets of commuting Pauli strings, since all the strings inside the same set can be measured at once. This strategy reduces the number of Trotter steps we can encode into n_a auxiliary qubits from n to n', but reduces the computational cost from exponential to polynomial in the number of physical spins. In Sec. III we show how to implement this strategy for the physical system under consideration.

D. Dynamical quantum phase transitions

Given a quantum system governed by the Hamiltonian $\hat{H}$ with initial state $|\psi(0)\rangle$, the Loschmidt echo is defined by

$$L(t) \equiv |\langle\psi(0)|e^{-i\hat{H}t}|\psi(0)\rangle|^2 = |\langle\psi(0)|\psi(t)\rangle|^2. \tag{10}$$

Loschmidt echoes are important quantities in many-body theory and appear in various contexts such as quantum chaos [56,57] or Schwinger's particle production mechanism [58,59]. In particular, we will consider the measurement of Loschmidt echoes for the identification of dynamical quantum phase transitions (DQPT) [49,60]. Because the variational history state encodes the superposition of all different time-evolved physical states $|\psi(t)\rangle$, we will show in the following that it is computationally cheap to evaluate the Loschmidt echo on it.

Dynamical phase transitions can be identified by a nonanalytic behavior of the Loschmidt echo and of its rate function $\lambda(t)$,

$$\lambda(t) = -\lim_{D\to\infty} \frac{1}{D}\log\left[L(t)\right], \tag{11}$$

where D is the number of degrees of freedom in our quantum system. Such phase transitions have been identified in many quantum systems [49] and also observed in experiments performed on analog quantum simulators [61–63].

In the following, we will show how to use the VFK method to study these phenomena. Assuming that the variational parameters of a circuit approximating the history state are obtained, we use an additional qubit to perform a Hadamard test [64] and measure the real and the imaginary part of $\langle\psi(t_i)|\psi(t_j)\rangle$ in order to calculate the Loschmidt echo. This only requires an additional qubit, and the gate overhead required to calculate the Loschmidt echo with VFK state is negligible with respect to the total number of gates of the variational state.

A more detailed explanation of the Hadamard test, as well as the complete circuit, can be found in Appendix D, while an application of this method is reported in Sec. III.

III. RESULTS

To demonstrate the viability of the VFK method, we consider the transverse-field Ising model on an open one-dimensional chain,

$$\hat{H} = J\sum_{i=0}^{n_s-1}\hat{\sigma}_i^z\hat{\sigma}_{i+1}^z + h\sum_{i=0}^{n_s}\hat{\sigma}_i^x \quad . \tag{12}$$

The first term accounts for interaction between spins while the latter represents a local and uniform magnetic field along the transverse direction x. For our simulations, we considered $J = \frac{1}{4}$, $h = 1$. We use a classical computer to simulate the quantum hardware in an ideal case, without noise sources and with full access to the state vector produced by the quantum circuit (state-vector simulations). The simulations have been performed both in PYTHON, using IBM's open-source library for quantum computing, Qiskit [65], and in JULIA [66], with the Yao.jl [67] and PastaQ [68] frameworks. The code can be found in Refs. [69,70].

We considered a variational ansatz of the form

$$\hat{V}(\theta) = \prod_{l=1}^{d}\left[\prod_{a\in A}\left(\prod_{\substack{i\neq j\\ i,j\in P}}\hat{G}_{ij,l}\prod_{p\in P}\hat{G}_{ap,l}\right)\right], \tag{13}$$

where we denoted the set of qubits encoding the physical system P and the set of auxiliary qubits A, while $G_{ij,l}$ is a parameterized gate of the form

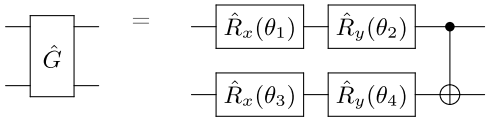

The total number of blocks, or depth, is d. The total number of variational parameters is then given by

$$n_{pars} = 2dn_a\left(n_s^2 + n_s\right), \tag{14}$$

where n_s and n_a indicate the number of spin and auxiliary qubits, respectively.

The Ising Hamiltonian in Eq. (12) has two sets of noncommuting operators $H_X = \sum_{i=0}^{n_s}\hat{\sigma}_i^x$ and $H_{ZZ} = \sum_{i=0}^{n_s-1}\hat{\sigma}_i^z\hat{\sigma}_{i+1}^z$. We make use of the strategy presented in Sec. II C in order to have a polynomial cost. We build the Feynman-Kitaev Hamiltonian by applying $U_X(dt) = \exp[-iH_X dt]$ at even clock values and $U_{ZZ}(dt) = \exp[-iH_{ZZ}dt]$ at odd ones. The new amount of Trotter step that can be encoded in n_a auxiliary qubits will be $n' = \frac{n}{2}$.

First, we considered a system with $n_s = 6$ spins and up to $n_a = 6$ auxiliary qubits for a total simulation time $T_e = 3$. We used the variational wave functions obtained with VFK to estimate expectation values of physical quantities as indicated in Eq. (8). In particular, we evaluated the total magnetization along the z axis,

$$\sigma^z = \frac{1}{n_s}\sum_{i=1}^{n_s}\sigma_i^z, \tag{15}$$

through the entire time evolution. To assess the accuracy of these variational history states obtained with the VFK method, we measured the infidelity $1 - F_{\text{VFK}}$ with respect to Trotter-Suzuki wave functions. For every simulated time t_i, we prepared the Trotter-Suzuki state $|\psi_i^{TS}\rangle = \hat{U}_{TS}^i(dt)|\psi(0)\rangle$ with $dt = \frac{T_e}{2^{n_a-1}}$ and evaluated the infidelity with the VFK history state projected onto the $|i\rangle$ subspace. The results are reported in Fig. 2.

Increasing the number of auxiliary qubits while keeping the total simulation time T_e fixed decreases the size of a single Trotter step, decreasing also the error with respect to the exact state. We remark that, if the variational ansatz is able to reproduce exactly the history state, the variational history

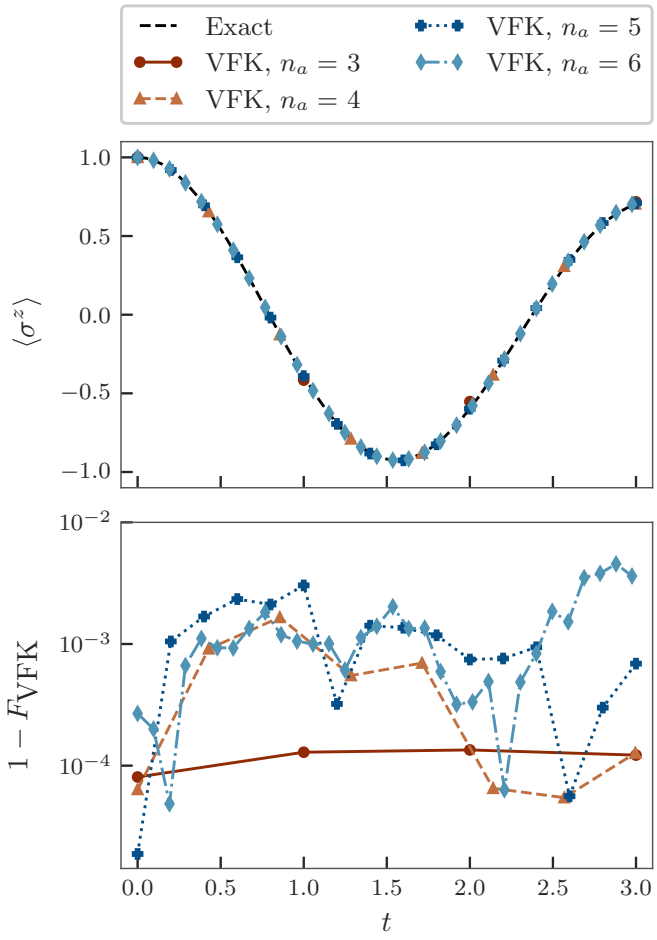

FIG. 2. Magnetization (top) and infidelities (bottom) measured on the VFK history state. We considered a system of $n_s = 6$ spins initialized in $|0\rangle^{\otimes 6}$ and different auxiliary qubits n_a for a simulation time $T_e = 3.0$. F_{VFK} at time t_i indicates the fidelity measured between the Trotter-Suzuki state with i steps and the VFK state projected on the $|i\rangle$ subspace.

state can be as accurate as the corresponding Trotter-Suzuki approximation.

We run multiple simulations for varying system and clock sizes $n_s, n_a \in [2, 3, 4, 5, 6]$. The ground-state optimization is performed using the variational quantum eigensolver (VQE) algorithm and the Adam optimizer [71]. The time evolution unitaries in the target Feynman-Kitaev Hamiltonian are smoothly varied from $\hat{U}(dt = 0)$ to $\hat{U}(dt = T_e/2^{n_a - 1})$ in order to help the convergence of the method (see Appendix B for additional details).

During the optimization we monitor the energy of the state, which we showed to bound the infidelity with respect to the target state. Once it gets below a certain threshold, we stop the optimization and consider that we have reached convergence. Since the energy of the first excited states of the Feynman-Kitaev Hamiltonian decreases as the number of auxiliary qubits increases, the threshold is chosen to be $10^{-2} \times E_1$, where E_1 indicates the energy of the first excited state. As indicated in Ref. [38], E_1 can be derived analytically from a unitarily equivalent Hamiltonian and its value is $E_1 = 1 - \cos(\pi/2^{n_a})$. For this reason, we are able to use E_1 as convergence threshold.

The complexity of the optimization procedure increases with the number of auxiliary qubits, however we are able to reach convergence by increasing the ansatz depth d. This is consistent with the fact that preparing the *exact history state* would require an exponentially deep circuit with the clock system size. In Fig. 3 we report the final energies obtained as a function of the ansatz depth. For comparison, in Appendix C we report the infidelities with respect to the exact ground state for the same calculations.

Then, we considered the smallest depth necessary to reach convergence and compared the number of two-qubit gates needed by the variational circuit with the number of two-qubit gates needed by a standard Trotter-Suzuki circuit with the same number of time steps. The results are indicated in Fig. 4. We only report the comparison for two-qubit gates and not for one-qubit gates because the latter are usually not a bottleneck in noisy intermediate-scale quantum (NISQ) devices.

In Fig. 4 we show that the VFK history state has an overhead compared to Trotter if few time steps are considered, but as the number of time steps is increased, the VFK method has a favorable scaling. Moreover, the VFK history state contains more information than the state obtained at the end of the Trotter evolution, which can be used, for example, to compute Loschmidt echoes.

In this regard, we show that the VFK variational wave function can be used to study dynamical quantum phase transitions. We still consider the transverse-field Ising model with $J = 1/4$ and $h = 1$. As the equilibrium model exhibits a quantum phase transition in the ground state when going from $h < J$ to $h > J$, a dynamical quantum phase transition is known to appear if the system is quenched from one region to the other [49].

We consider a system initialized at $|\psi(0)\rangle = |0\rangle^{\otimes n_s}$, the ground state of the Hamiltonian for $h = 0$, and we then compute the VFK history state using the same procedure described before for $T_e = 3$, $h = 1$, and varying system sizes. After determining the optimal parameters, we used the Hadamard test to evaluate the rate function of the Loschmidt echo as described in Appendix D. In Fig. 5 we show that a nonanalytic behavior appears as the system size grows. We are able to improve the time resolution by increasing the number of auxiliary qubits. As the number of spins approaches the thermodynamic limit, the qubit overhead required to characterize the cusp becomes negligible.

Finally, we investigate the algorithm performance in the presence of noise. We follow the noise model proposed by Kandala *et al.* in Ref. [47], where the effects of decoherence are approximated by an amplitude damping and dephasing channel acting after each fundamental gate on the system density matrix ρ as

$$\begin{aligned} \rho &\to E_0^a \rho E_0^{a\dagger} + E_1^a \rho E_1^{a\dagger}, \\ \rho &\to E_0^d \rho E_0^{d\dagger} + E_1^d \rho E_1^{d\dagger} \end{aligned} \tag{16}$$

with

$$E_0^a = \begin{bmatrix} 1 & 0 \\ 0 & \sqrt{1-p^a} \end{bmatrix}, \quad E_1^a = \begin{bmatrix} 0 & \sqrt{p^a} \\ 0 & 0 \end{bmatrix} \tag{17}$$

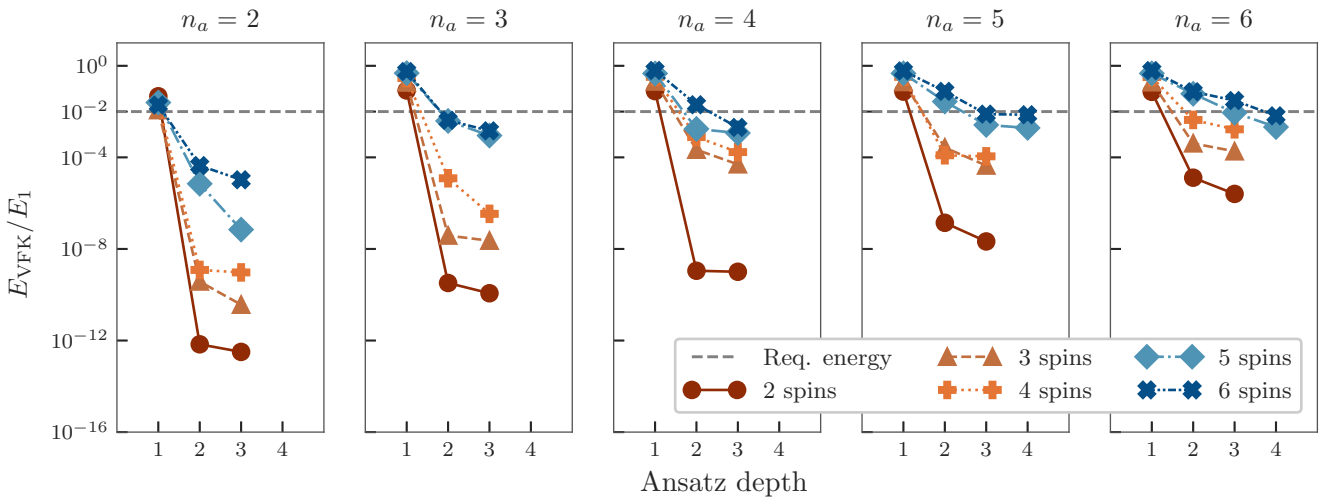

FIG. 3. Final energy obtained with the VFK algorithm (E_{VFK}) over the energy of the first excited state (E_1) obtained using a classical simulator. The plot shows the final energy obtained for a system of n_s spins and 2^{n_a-1} time steps as a function of the depth of ansatz in Eq. (13). The gray, dashed lines indicate the energies we require to consider the VFK converged. We fixed the simulation time $T_e = 3.0$. In this case, increasing the number of auxiliary qubits will reduce the time step and the Trotter-Suzuki approximation error, accordingly. The corresponding fidelities can be found in Appendix C.

and

$$E_0^d = \begin{bmatrix} 1 & 0 \\ 0 & \sqrt{1-p^d} \end{bmatrix}, \quad E_1^d = \begin{bmatrix} 0 & 0 \\ 0 & \sqrt{p^d} \end{bmatrix}. \tag{18}$$

The fundamental gates are taken to be CNOT, $\hat{R}_x$, $\hat{R}_y$, and $\hat{R}_z$; all other gates, such as the $\hat{R}_{zz}$ used in the Trotter circuit, are decomposed into a sequence of those gates. The one- and two-qubit error rates $p_1^{a,d}$ and $p_2^{a,d}$ are estimated from quantum processing unit (QPU) data such as the relaxation and dephasing time available in Refs. [1,4]. More details on the estimation of error rates can be found in Appendix E.

In Fig. 6 we compare the mean fidelity F_{VFK} obtained from the VFK calculation on the noisy system of $n_s = 2$ spins and different n_a against the mean fidelity of the Trotter evolution F_{TS} [we take the fidelity to be $F(\rho,\sigma) = [\mathrm{Tr}(\sqrt{\sqrt{\rho}\sigma\sqrt{\rho}})]^2$,

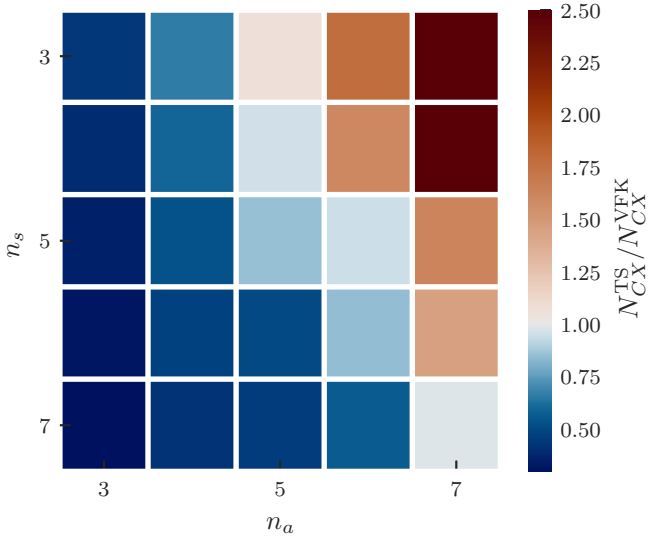

FIG. 4. Comparison between two-qubit gates required by the Trotter-Suzuki circuit ($N_{\mathrm{CX}}^{\mathrm{TS}}$) and by the variational ansatz ($N_{\mathrm{CX}}^{\mathrm{VFK}}$), given the same system size and Trotter steps. $N_{\mathrm{CX}}^{\mathrm{VFK}}$ corresponds to the minimal circuit required to make VFK converge and depends on ansatz type and depth. $N_{\mathrm{CX}}^{\mathrm{TS}}$ is fixed, given the system size and number of steps. We considered the ansatz in Eq. (13) and a simulation time $T_e = 3.0$.

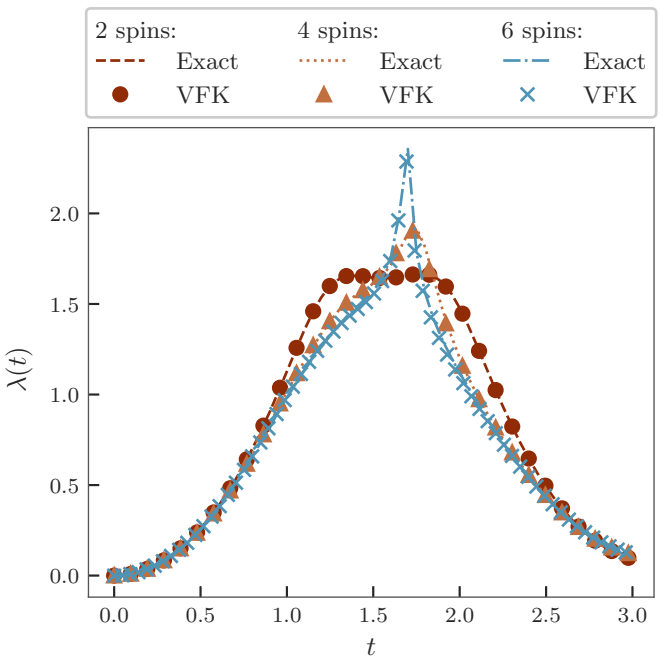

FIG. 5. Rate function of the Loschmidt echo in the transverse-field Ising model measured using the VFK variational state. The plot shows a dynamical phase transition for an open chain initialized in the $|0\rangle^{\otimes n_s}$ state and evolved under the Hamiltonian in Eq. (12). The nonanalyticity appears when the number of spins is increased. We considered a number of auxiliary qubits $n_a = 6$ for $n_s = 2, 4$ and $n_a = 7$ for $n_s = 6$.

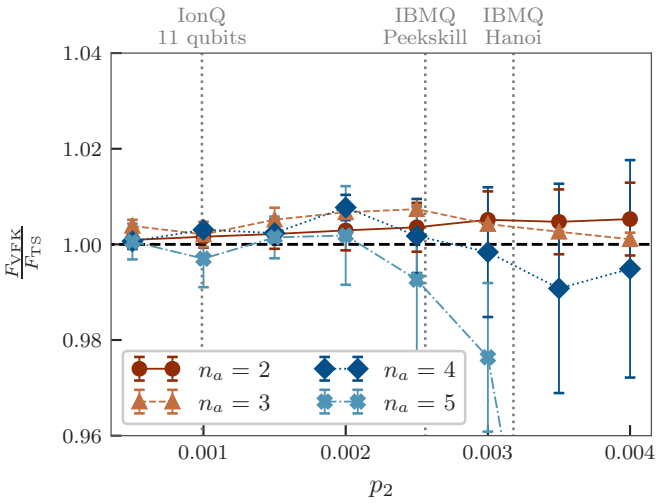

FIG. 6. Comparison between the mean infidelity of noisy VFK and Trotter-Suzuki circuits through a time evolution to $T_e = 3.0$. Markers indicate the mean value, while the bars show the standard deviation over a time evolution. We fixed the error probability for single-qubit gates $p_1 = 2 \times 10^{-4}$. We considered a system with $n_s = 2$ and a different number of auxiliary qubits n_a, and Trotter steps are varied accordingly. The horizontal line indicates equal mean fidelity between VFK and Trotter-Suzuki circuits. Vertical lines indicate the mean p_2 error probability for reference devices.

where ρ, σ are two density matrices]. We study how their ratio $F_{\rm VFK}/F_{\rm TS}$ varies as a function of different two-qubit error rates $p_2^a = p_2^d = p_2$, while keeping the single-qubit error rate constant to an average value $p_1^a = p_1^d = p_1 = 2 \times 10^{-4}$ that is consistent with real-world devices. This approach is motivated by the fact that today's devices are mainly limited in the fidelity they can achieve when performing two-qubit operations.

The plot indicates comparable performances between the two methods, with an advantage of VFK for $n_a = 2, 3$. As the number of auxiliary qubits is increased to $n_a = 4, 5$, the VFK optimization must converge towards smaller values of the energy in order to give sensible results. However, at higher error rates we were not able to successfully optimize the variational parameters, which can be seen in the figure by the fact that the performance of the VFK method then degrades. To give a better idea of where today's QPUs stand, some vertical lines represent the mean values of p_2 for commercially available devices, which shows that ion-based setups have a low-enough error rate and could be able to use the VFK algorithm efficiently already today.

IV. CONCLUSIONS AND OUTLOOK

In this work we showed a strategy to study dynamical properties of a quantum system using variational ground-state quantum algorithms. Our method, which we called variational Feynman-Kitaev (VFK), combines the Feynman-Kitaev Hamiltonian together with existing variational ground-state methods in order to study dynamical systems with the limited resources available on today's NISQ devices.

First, we showed how the Feynman-Kitaev Hamiltonian can be efficiently implemented on a quantum computer using a binary encoding for the auxiliary system and the Trotter-Suzuki approximation for the time evolution operator. Then, we demonstrated our method studying the transverse-field Ising model and showing that it scales favorably compared to a Trotter-Suzuki evolution when many time steps are needed. We investigated the convergence of the algorithm as the number of spins and auxiliary qubits increases and compared the final circuits with the corresponding Trotter-Suzuki approximation. Considering a noise model accounting for decoherence, we assessed that our algorithm yields slightly better results than a plain Trotter evolution when the two-qubit error rate is not too detrimental. As analyzed in Ref. [46], variational methods are robust against certain types of quantum errors, a promising feature for future hardware demonstrations. Finally, we showed that it is possible to exploit the structure of the VFK history state to measure dynamical quantities such as the Loschmidt echo efficiently, and gave an example of how to detect dynamical quantum phase transitions in the transverse-field Ising model.

As a future research direction, we believe that it would be of interest to investigate the application of the VFK method to other physical systems, as well as its application to estimate quantities that are not easily accessible via standard Trotterization. Similarly to all other variational algorithms, the choice of the right ansatz is fundamental for the algorithm to succeed. In the ansatz we proposed, the gates required between auxiliary and system qubits currently limit the implementation on hardware. However, we envision application of the method in devices with high qubit connectivity. Moreover, we showed that once the variational history state is obtained, it has applications beyond the evaluation of expectation values of time-dependent observables.

The code used to run the simulations is open source and can be found in Refs. [69,70].

ACKNOWLEDGMENT

This research was supported by the NCCR MARVEL, a National Centre of Competence in Research, funded by the Swiss National Science Foundation (Grant No. 205602).

APPENDIX A: COMPARISON WITH PROJECTED VARIATIONAL QUANTUM DYNAMICS

In this Appendix we compare the VFK method to the p-VQD method presented in Ref. [29]. We consider the same transverse-field Ising model (TFIM) in Eq. (12) and the same parameters. The p-VQD variational state is prepared using the ansatz presented in Ref. [29]. We define the mean integrated infidelity

$$\delta_F(T_e) = \frac{1}{T_e}\int_{t=0}^{T_e}(1 - |\langle\psi_{TS}(t)|\psi_{\theta_t}\rangle|^2)dt = \frac{\Delta_F(T_e)}{T_e}, \quad \text{(A1)}$$

where $|\psi_{TS}(t)\rangle$ is the Trotter-Suzuki state prepared at time t, while $|\psi_{\theta_t}\rangle$ indicates the variational state that approximates it. In the VFK method, the variational history state $|\Psi_\theta\rangle$ is prepared and projected onto the $|t\rangle$ subspace before calculating the fidelity. We fix a total simulation time T_e, and the number of auxiliary qubits in the VFK method determine the number of time steps for both methods. Given that, differently from

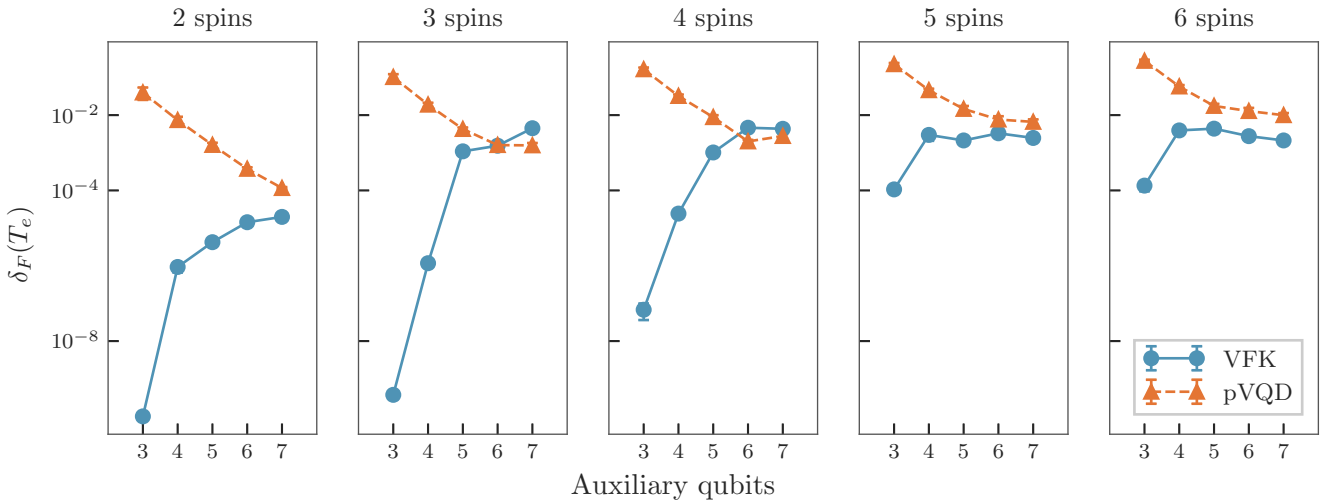

FIG. 7. Mean infidelity over an entire time evolution as a function of the number of spins and auxiliary qubits. The plot compares the mean infidelity between the variational state obtained with VFK (after projecting to $|t\rangle$ subspace) or p-VQD and the exact state. For the VQE we used the ansatz in Eq. (13), while for p-VQD we use the alternating rotations ansatz presented in Ref. [29]. We considered a total simulation time $T_e = 3.0$ and a number of optimization steps comparable between the two methods. The analysis is performed using a state-vector simulator and the Adam optimizer for both methods.

VFK, the variational wave function prepared by the p-VQD algorithm encodes the evolution of the quantum state only at a certain time t, the ansatze used in the two methods are different. For VFK, the ansatz is the same one presented in Eq. (13), with depth of converged calculations in Fig. 3. For p-VQD, we use the same ansatz presented in Ref. [29] with depth $d = 3$, resulting in a total number of $d[n_s + (n_s - 1)] + n_s = 7n_s - 3$ free parameters.

We use the Adam optimizer and a comparable number of optimization steps. Results of this comparison are shown in Fig. 7.

When the number of time steps is small, the infidelity of the VFK method is lower. If we choose a time step small enough, we are able to improve the accuracy of the p-VQD method, thanks to parameter optimization at every time step. Provided a converged optimization is used, they are expected to converge to the same mean integrated infidelity in the limit of infinite time steps.

APPENDIX B: OPTIMIZATION STRATEGY

As a variational algorithm, optimization of the wave function using VQE can be hindered by local minima or the presence of barren plateaus [72–74]. In particular, the definition of the cost function in terms of global observables leads to the emergence of such plateaus even when $V(\theta)$ is a shallow circuit [74]. To improve the optimization procedure, we devise a specific strategy. Consider $dt = 0$: in this case the history state has the form

$$|\Psi_0\rangle = \frac{1}{\sqrt{n+1}} \sum_{i=0}^{n} |\psi(0)\rangle|i\rangle. \tag{B1}$$

When dt is infinitesimal, the history state $|\Psi\rangle$ is infinitesimally close to $|\Psi_0\rangle$. Assuming $|\psi(0)\rangle$ is a simple state to prepare or, equivalently, that we have an efficient approximation to it, we start with the circuit in the state $|\Psi_0\rangle$ and initialize the variational gates as identity operators. Then, we substitute every $\hat{U}(dt)$ in the Feynman-Kitaev Hamiltonian with its k-root $\sqrt[k]{\hat{U}(dt)} = \hat{U}(dt/k)$. Considering large-enough k, we can start the optimization close to the optimum. Finally, we optimize the wave function for decreasing k until $k = 1$ and the targeted clock Hamiltonian is obtained. In general, every function $f(dt, k)$ can be considered and the Feynman-Kitaev Hamiltonian built upon $\hat{U}[f(dt, k)]$, e.g., $f(dt, k) = dt\frac{k}{k_0}$ with $k \in \{1, \ldots, k_0\}$ and k_0 an arbitrary large number.

APPENDIX C: FIDELITY OF THE VQE CALCULATIONS

In this Appendix we show the fidelity between the variational state obtained with the VFK algorithm and the corresponding exact history state. As explained in Sec. II A, the fidelity is upper bounded by the normalized energy. Indeed, given a state $|\phi\rangle = \sqrt{1-\epsilon^2}|\Psi\rangle + \epsilon|\delta\rangle$ close to the target state $|\Psi\rangle$, where $\epsilon \approx 0$, $\langle\Psi|\delta\rangle = 0$, we can calculate its fidelity and energy as a function of ϵ.

In particular, we obtain that $1 - F(\phi, \Psi) = \epsilon^2$ and $E(|\phi\rangle) = \epsilon^2 E(|\delta\rangle)$, where we defined $F(\phi, \Psi) = |\langle\phi|\Psi\rangle|^2$ and to calculate $E(|\phi\rangle)$ we considered that $E(|\Psi\rangle) = 0$ by construction. Given that $|\delta\rangle$ is orthogonal to $|\Psi\rangle$, $E(|\delta\rangle) \geqslant E_1$, where E_1 is the energy of the first excited state. For this reason, we can conclude that the infidelity is upper bounded by the energy normalized by E_1, which can be calculated analytically, as shown in Ref. [38]. In Fig. 8 we report the infidelities for states whose energy is shown in Fig. 3

APPENDIX D: MEASURING LOSCHMIDT ECHOES

In this Appendix, we illustrate how to extend the VFK circuit in order to measure Loschmidt echoes. Consider the overlap between the system quantum state evolved at two different times t_i and t_j, namely, $\langle\psi(t_i)|\psi(t_j)\rangle$. In general, this quantity is complex, therefore we have to perform a Hadamard test to evaluate its real and imaginary part. In the following,

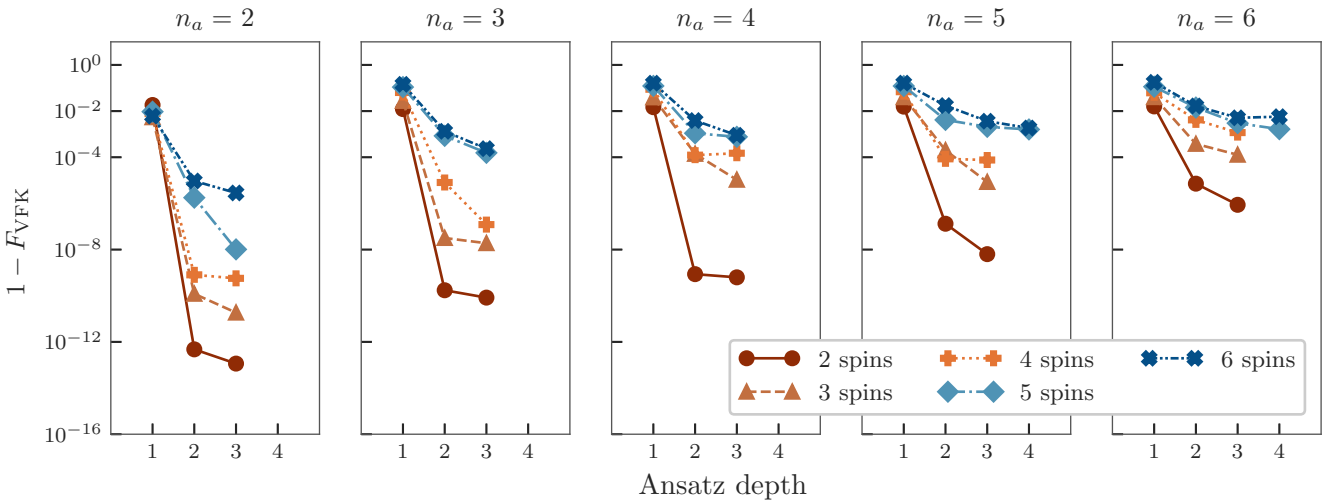

FIG. 8. Final infidelities of the states obtained with the VFK algorithm ($1 - F_{\mathrm{VFK}}$) using a classical simulator with respect to the exact history state. The plot reports the infidelities corresponding to the calculations presented in Fig. 3.

we describe how to measure the real part; the same procedure applies for the imaginary part, with a slight modification.

First, we define the time-swap operator as

$$\hat{\mathrm{T}}_{\mathrm{SWAP}}(t_i, t_j) = \bigotimes_{k \in T_{ij}} \hat{\sigma}_k^x, \tag{D1}$$

where T_{ij} indicates the set of bits that differs in the bit string encoding of t_i and t_j. We use the set of parameters obtained with the VFK method to initialize the variational circuit $V(\theta)$. We control the action of the time-swap operator over the clock system using an additional auxiliary qubit initialized in $|+\rangle = \frac{|0\rangle+|1\rangle}{\sqrt{2}} = H|0\rangle$. In the following, we will refer to the qubits of the auxiliary clock system as the clock qubits, to distinguish them from the auxiliary qubit added to perform the Hadamard test. Then, we apply again a Hadamard gate to the auxiliary qubit and we measure the auxiliary and the clock qubits. We postselect the measurements in which the measurement of the clock system returns the binary string corresponding to t_i (or t_j). We indicate the number of postselected measurements with the auxiliary qubit in 0 (1) as N_0 (N_1).

Finally, the real part of the overlap will be

$$\langle \psi(t_i)|\psi(t_j)\rangle = 2^{n_a} \frac{N_0 - N_1}{N_{\mathrm{shots}}}, \tag{D2}$$

where N_{shots} indicates the number of times the system has been prepared and measured, while the prefactor 2^{n_a} is required for the normalization of the history state. Considered a system with two system qubits and a single clock qubit, the final circuit to measure the real part of $\langle \psi(t_0)|\psi(t_1)\rangle$ has the form

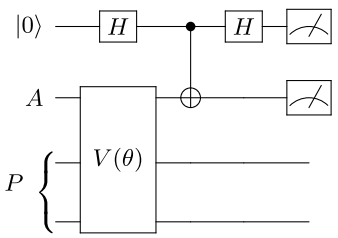

where P indicates the two system qubits and A the clock qubit. To measure the imaginary part of the overlap, the same procedure applies, with the auxiliary qubit initialized in $\frac{|0\rangle - i|1\rangle}{\sqrt{2}} = HS^\dagger|0\rangle$.

APPENDIX E: NOISE MODEL FOR THE NUMERICAL EXPERIMENTS

In this Appendix, we describe how we included decoherence effects in the numerical simulations shown in Fig. 6. As indicated in the main text, we followed the noise model proposed by Kandala *et al.* in Ref. [47], where the effects of decoherence are approximated by the successive application of an amplitude damping and dephasing channel acting after each gate on the system density matrix

$$\begin{aligned} \rho &\to E_0^a \rho E_0^{a\dagger} + E_1^a \rho E_1^{a\dagger}, \\ \rho &\to E_0^d \rho E_0^{d\dagger} + E_1^d \rho E_1^{d\dagger} \end{aligned} \tag{E1}$$

with

$$\begin{aligned} E_0^a &= \begin{bmatrix} 1 & 0 \\ 0 & \sqrt{1-p^a} \end{bmatrix}, \quad E_1^a = \begin{bmatrix} 0 & \sqrt{p^a} \\ 0 & 0 \end{bmatrix} \quad \text{and} \\ E_0^d &= \begin{bmatrix} 1 & 0 \\ 0 & \sqrt{1-p^d} \end{bmatrix}, \quad E_1^d = \begin{bmatrix} 0 & 0 \\ 0 & \sqrt{p^d} \end{bmatrix}. \end{aligned} \tag{E2}$$

The error rates p^a and p^d can be determined from actual device data. In particular, we have

$$p^a = 1 - e^{-\tau/T_1}, \quad p_g^d = 1 - e^{-2\tau/T_\phi}, \tag{E3}$$

TABLE I. Average coherence values and gate times of the devices indicated in Fig. 6, as of March 2022.

Device	T_1 (μs)	T_2 (μs)	τ_2 (μs)	τ_1 (μs)
IBMQ Peekskill	250.12	242.82	0.420571	0.0035
IBMQ Hanoi	160.64	144.7	0.318603	0.0035
IonQ 11 qubits	$>10^7$	2×10^5	210	10

where T_1 is the relaxation time of the qubit, τ is the gate time, and $T_\phi = 2T_1T_2/(2T_1 - T_2)$, given T_2 as the coherence time of the qubit. When the time of a single- or two-qubit gate is substituted in τ, we obtain $p_1^{a,d}$ and $p_2^{a,d}$, respectively. We used data found in Refs. [1,4] to estimate an average value of $p_1^{a,d}$ and a range of $p_2^{a,d}$ to analyze in our simulations. Finally, in order to simplify the comparison in Fig. 6, we considered $p^a = p^d$ for both single- or two-qubit gates. This approximation holds when $T_1 \approx T_2$, which is true on an average basis for superconducting devices [1].

For completeness, we report in Table I the data of the devices indicated in Fig. 6.

[1] IBM, IBM Quantum services (Accessed March 2022)

[2] Google, Google AI Quantum hardware (Accessed March 2022).

[3] K. M. Beck, S. Debnath, J. M. Amini, Y. Nam, N. Grzesiak, J.-S. Chen, N. C. Pisenti, M. Chmielewski, C. Collins, K. M. Hudek *et al.*, Benchmarking an 11-qubit quantum computer, Nat. Commun. **10**, 5464 (2019).

[4] IonQ, IonQ devices and providers (Accessed March 2022).

[5] P. Shor, Algorithms for quantum computation: Discrete logarithms and factoring, in *Proceedings of the 35th Annual Symposium on Foundations of Computer Science* (IEEE Comput. Soc. Press, Washington, DC, 1994).

[6] L. K. Grover, A fast quantum mechanical algorithm for database search, in *Proceedings of the 28th Annual ACM Symposium on Theory of Computing*, STOC '96 (Association for Computing Machinery, New York, 1996), p. 212.

[7] G. E. Santoro and E. Tosatti, Optimization using quantum mechanics: Quantum annealing through adiabatic evolution, J. Phys. A: Math. Gen. **39**, R393 (2006).

[8] I. Kassal, S. P. Jordan, P. J. Love, M. Mohseni, and A. Aspuru-Guzik, Polynomial-time quantum algorithm for the simulation of chemical dynamics, Proc. Natl. Acad. Sci. USA **105**, 18681 (2008).

[9] I. M. Georgescu, S. Ashhab, and F. Nori, Quantum simulation, Rev. Mod. Phys. **86**, 153 (2014).

[10] R. P. Feynman, Simulating physics with computers, Int. J. Theor. Phys. **21**, 467 (1982).

[11] S. Lloyd, Universal quantum simulators, Science **273**, 1073 (1996).

[12] D. S. Abrams and S. Lloyd, Simulation of Many-Body Fermi Systems on a Universal Quantum Computer, Phys. Rev. Lett. **79**, 2586 (1997).

[13] C. Cade, L. Mineh, A. Montanaro, and S. Stanisic, Strategies for solving the Fermi-Hubbard model on near-term quantum computers, Phys. Rev. B **102**, 235122 (2020).

[14] Google AI Quantum and collaborators, Observation of separated dynamics of charge and spin in the Fermi-Hubbard model, arXiv:2010.07965.

[15] Y. Cao, J. Romero, J. P. Olson, M. Degroote, P. D. Johnson, M. Kieferová, I. D. Kivlichan, T. Menke, B. Peropadre, N. P. D. Sawaya, S. Sim, L. Veis, and A. Aspuru-Guzik, Quantum chemistry in the age of quantum computing, Chem. Rev. **119**, 10856 (2019).

[16] B. Bauer, S. Bravyi, M. Motta, and G. K.-L. Chan, Quantum algorithms for quantum chemistry and quantum materials science, Chem. Rev. **120**, 12685 (2020).

[17] N. Sheng, C. Vorwerk, M. Govoni, and G. Galli, Quantum embedding theories to simulate condensed systems on quantum computers, arXiv:2105.04736.

[18] L. Bassman, M. Urbanek, M. Metcalf, J. Carter, A. F. Kemper, and W. A. de Jong, Simulating quantum materials with digital quantum computers, Quantum Sci. Technol. **6**, 043002 (2021).

[19] A. M. Childs, D. Maslov, Y. Nam, N. J. Ross, and Y. Su, Toward the first quantum simulation with quantum speedup, Proc. Natl. Acad. Sci. USA **115**, 9456 (2018).

[20] R. Babbush, C. Gidney, D. W. Berry, N. Wiebe, J. McClean, A. Paler, A. Fowler, and H. Neven, Encoding Electronic Spectra in Quantum Circuits with Linear T Complexity, Phys. Rev. X **8**, 041015 (2018).

[21] Y. Nam and D. Maslov, Low-cost quantum circuits for classically intractable instances of the Hamiltonian dynamics simulation problem, npj Quantum Inf. **5**, 44 (2019).

[22] M. Motta, E. Ye, J. R. McClean, Z. Li, A. J. Minnich, R. Babbush, and G. K.-L. Chan, Low rank representations for quantum simulation of electronic structure, npj Quantum Inf. **7**, 83 (2021).

[23] A. Peruzzo, J. McClean, P. Shadbolt, M.-H. Yung, X.-Q. Zhou, P. J. Love, A. Aspuru-Guzik, and J. L. O'Brien, A variational eigenvalue solver on a photonic quantum processor, Nat. Commun. **5**, 4213 (2014).

[24] Y. Li and S. C. Benjamin, Efficient Variational Quantum Simulator Incorporating Active Error Minimization, Phys. Rev. X **7**, 021050 (2017).

[25] M. Motta, C. Sun, A. T. K. Tan, M. J. O'Rourke, E. Ye, A. J. Minnich, F. G. S. L. Brandão, and G. K.-L. Chan, Determining eigenstates and thermal states on a quantum computer using quantum imaginary time evolution, Nat. Phys. **16**, 205 (2020).

[26] P. J. Ollitrault, A. Kandala, C.-F. Chen, P. K. Barkoutsos, A. Mezzacapo, M. Pistoia, S. Sheldon, S. Woerner, J. M. Gambetta, and I. Tavernelli, Quantum equation of motion for computing molecular excitation energies on a noisy quantum processor, Phys. Rev. Res. **2**, 043140 (2020).

[27] X. Yuan, S. Endo, Q. Zhao, Y. Li, and S. C. Benjamin, Theory of variational quantum simulation, Quantum **3**, 191 (2019).

[28] M. Cerezo, A. Arrasmith, R. Babbush, S. C. Benjamin, S. Endo, K. Fujii, J. R. McClean, K. Mitarai, X. Yuan, L. Cincio, and P. J. Coles, Variational quantum algorithms, Nat. Rev. Phys. **3**, 625 (2021).

[29] S. Barison, F. Vicentini, and G. Carleo, An efficient quantum algorithm for the time evolution of parameterized circuits, Quantum **5**, 512 (2021).

[30] S.-H. Lin, R. Dilip, A. G. Green, A. Smith, and F. Pollmann, Real- and imaginary-time evolution with compressed quantum circuits, PRX Quantum **2**, 010342 (2021).

[31] F. Barratt, J. Dborin, M. Bal, V. Stojevic, F. Pollmann, and A. G. Green, Parallel quantum simulation of large systems on small NISQ computers, npj Quantum Inf. **7**, 79 (2021).

[32] M. Otten, C. L. Cortes, and S. K. Gray, Noise-resilient quantum dynamics using symmetry-preserving ansatzes, arXiv:1910.06284.

[33] C. Cîrstoiu, Z. Holmes, J. Iosue, L. Cincio, P. J. Coles, and A. Sornborger, Variational fast forwarding for quantum simulation beyond the coherence time, npj Quantum Inf. **6**, 82 (2020).

[34] B. Commeau, M. Cerezo, Z. Holmes, L. Cincio, P. J. Coles, and A. Sornborger, Variational Hamiltonian diagonalization for dynamical quantum simulation, arXiv:2009.02559.

[35] K. Bharti and T. Haug, Quantum-assisted simulator, Phys. Rev. A **104**, 042418 (2021).

[36] M. Benedetti, M. Fiorentini, and M. Lubasch, Hardware-efficient variational quantum algorithms for time evolution, Phys. Rev. Res. **3**, 033083 (2021).

[37] R. P. Feynman, Quantum mechanical computers, Opt. News **11**, 11 (1985).

[38] A. Y. Kitaev, A. H. Shen, and M. N. Vyalyi, *Classical and Quantum Computation* (American Mathematical Society, Providence, RI, 2002).

[39] L. Caha, Z. Landau, and D. Nagaj, Clocks in Feynman's computer and Kitaev's local Hamiltonian: Bias, gaps, idling, and pulse tuning, Phys. Rev. A **97**, 062306 (2018).

[40] J. Bausch and E. Crosson, Analysis and limitations of modified circuit-to-Hamiltonian constructions, Quantum **2**, 94 (2018).

[41] V. Giovannetti, S. Lloyd, and L. Maccone, Quantum time, Phys. Rev. D **92**, 045033 (2015).

[42] J. R. McClean, J. A. Parkhill, and A. Aspuru-Guzik, Feynman's clock, a new variational principle, and parallel-in-time quantum dynamics, Proc. Natl. Acad. Sci. USA **110**, E3901 (2013).

[43] D. G. Tempel and A. Aspuru-Guzik, The Kitaev–Feynman clock for open quantum systems, New J. Phys. **16**, 113066 (2014).

[44] J. R. McClean and A. Aspuru-Guzik, Clock quantum Monte Carlo technique: An imaginary-time method for real-time quantum dynamics, Phys. Rev. A **91**, 012311 (2015).

[45] J. Watkins, N. Wiebe, A. Roggero, and D. Lee, Time-dependent Hamiltonian simulation using discrete clock constructions, arXiv:2203.11353.

[46] J. R. McClean, J. Romero, R. Babbush, and A. Aspuru-Guzik, The theory of variational hybrid quantum-classical algorithms, New J. Phys. **18**, 023023 (2016).

[47] A. Kandala, A. Mezzacapo, K. Temme, M. Takita, M. Brink, J. M. Chow, and J. M. Gambetta, Hardware-efficient variational quantum eigensolver for small molecules and quantum magnets, Nature (London) **549**, 242 (2017).

[48] A. McLachlan, A variational solution of the time-dependent Schrodinger equation, Mol. Phys. **8**, 39 (1964).

[49] M. Heyl, Dynamical quantum phase transitions: a review, Rep. Prog. Phys. **81**, 054001 (2018).

[50] E. P. Jornan, *The Collected Works of Eugene Paul Wigner* (Springer, Berlin, 1993).

[51] S. B. Bravyi and A. Y. Kitaev, Fermionic quantum computation, Ann. Phys. **298**, 210 (2002).

[52] N. P. D. Sawaya, T. Menke, T. H. Kyaw, S. Johri, A. Aspuru-Guzik, and G. G. Guerreschi, Resource-efficient digital quantum simulation of *d*-level systems for photonic, vibrational, and spin-*s* Hamiltonians, npj Quantum Inf. **6**, 49 (2020).

[53] F. Gray, Pulse code communication, US Patent No. 2,632,058 (Mar. 1953).

[54] H. F. Trotter, Proc. Am. Math. Soc. **10**, 545 (1959).

[55] M. Suzuki, General theory of fractal path integrals with applications to many-body theories and statistical physics, J. Math. Phys. **32**, 400 (1991).

[56] A. Peres, Stability of quantum motion in chaotic and regular systems, Phys. Rev. A **30**, 1610 (1984).

[57] T. Gorin, T. Prosen, T. H. Seligman, and M. Žnidarič, Dynamics of Loschmidt echoes and fidelity decay, Phys. Rep. **435**, 33 (2006).

[58] J. Schwinger, On gauge invariance and vacuum polarization, Phys. Rev. **82**, 664 (1951).

[59] E. A. Martinez, C. A. Muschik, P. Schindler, D. Nigg, A. Erhard, M. Heyl, P. Hauke, M. Dalmonte, T. Monz, P. Zoller *et al.*, Real-time dynamics of lattice gauge theories with a few-qubit quantum computer, Nature (London) **534**, 516 (2016).

[60] M. Heyl, A. Polkovnikov, and S. Kehrein, Dynamical Quantum Phase Transitions in the Transverse-Field Ising Model, Phys. Rev. Lett. **110**, 135704 (2013).

[61] P. Jurcevic, H. Shen, P. Hauke, C. Maier, T. Brydges, C. Hempel, B. P. Lanyon, M. Heyl, R. Blatt, and C. F. Roos, Direct Observation of Dynamical Quantum Phase Transitions in an Interacting Many-Body System, Phys. Rev. Lett. **119**, 080501 (2017).

[62] N. Flaeschner, D. Vogel, M. Tarnowski, B. Rem, D.-S. Lühmann, M. Heyl, J. Budich, L. Mathey, K. Sengstock, and C. Weitenberg, Observation of dynamical vortices after quenches in a system with topology, Nat. Phys. **14**, 265 (2018).

[63] X. Nie, B.-B. Wei, X. Chen, Z. Zhang, X. Zhao, C. Qiu, Y. Tian, Y. Ji, T. Xin, D. Lu, and J. Li, Experimental Observation of Equilibrium and Dynamical Quantum Phase Transitions via Out-of-Time-Ordered Correlators, Phys. Rev. Lett. **124**, 250601 (2020).

[64] A. K. Ekert, C. M. Alves, D. K. L. Oi, M. Horodecki, P. Horodecki, and L. C. Kwek, Direct Estimations of Linear and Nonlinear Functionals of a Quantum State, Phys. Rev. Lett. **88**, 217901 (2002).

[65] M. S. Anis, H. Abraham, A. Offei, R. Agarwal, G. Agliardi, M. Aharoni, V. Ajith, I. Y. Akhalwaya, G. Aleksandrowicz, T. Alexander, M. Amy *et al.*, *Qiskit: An open-source framework for quantum computing* (Zenodo, 2019), doi: 10.5281/zenodo.2573505.

[66] J. Bezanson, A. Edelman, S. Karpinski, and V. B. Shah, Julia: A fresh approach to numerical computing, SIAM Rev. **59**, 65 (2017).

[67] X.-Z. Luo, J.-G. Liu, P. Zhang, and L. Wang, Yao.jl: Extensible, efficient framework for quantum algorithm design, Quantum **4**, 341 (2020).

[68] G. Torlai and M. Fishman, PastaQ: A package for simulation, tomography and analysis of quantum computers (2020), https://github.com/GTorlai/PastaQ.jl.

[69] S. Barison, StefanoBarison/Variational-Feynman-Kitaev: First release, Data Set and Code for VFK (Zenodo, 2022), doi: 10.5281/zenodo.7298514.

[70] S. Barison, F. Vicentini, I. Cirac, and G. Carleo, Variational dynamics as a ground-state problem on a quantum computer,, Data set and code for VFK, MaterialsCloud (2022), doi: 10.24435/materialscloud:xf-wj.

[71] D. P. Kingma and J. Ba, Adam: A method for stochastic optimization arXiv:1412.6980.

[72] J. R. McClean, S. Boixo, V. N. Smelyanskiy, R. Babbush, and H. Neven, Barren plateaus in quantum neural network training landscapes, Nat. Commun. **9**, 4812 (2018).

[73] E. Grant, L. Wossnig, M. Ostaszewski, and M. Benedetti, An initialization strategy for addressing barren plateaus in parametrized quantum circuits, Quantum **3**, 214 (2019).

[74] M. Cerezo, A. Sone, T. Volkoff, L. Cincio, and P. J. Coles, Cost function dependent barren plateaus in shallow parametrized quantum circuits, Nat. Commun. **12**, 1791 (2021).